Mineralogy of complex Co-Ni-Bi vein mineralization, Bieber deposit, Spessart, Germany

T. Wagner[1,2,*] and J. Lorenz[3]

[1] Mineralogisches Institut, Universität Würzburg, Am Hubland, D-97074 Würzburg, Germany
[2] Department of Earth and Planetary Sciences, McGill University, 3450 University Street, Montréal QC H3A 2A7, Canada
[3] Graslitzer Str. 5, D-63791 Karlstein am Main, Germany

ABSTRACT

Post-Variscan vein-type Co-Ni-Bi ores of the Bieber deposit, Spessart mountains, Germany, which are related to the Permian Kupferschiefer, have been investigated by ore microscopy, X-ray powder diffraction and electron-probe microanalysis. The samples contain a variety of ore minerals, notably skutterudite, native bismuth, cobaltite, alloclasite, niccolite, maucherite, gersdorffite, rammelsbergite/pararammelsbergite, safflorite, loellingite and emplectite. The ores display structures indicative of multiple brecciation and complex zoned arsenide assemblages. Three sequential stages of deposition are identified, which are (1) the Cu stage, (2) the main Co-Ni-Bi stage, and (3) the late stage. The arsenide minerals, notably skutterudite, diarsenides and sulpharsenides, show a large range of compositional variation in Co-Ni-Fe space. A relatively limited number of skutterudite and diarsenide compositions lie outside the compositional fields established in the literature. Skutterudite and diarsenides are characterized by a significant substitution of As by S up to 0.44 a.p.f.u. and 0.31 a.p.f.u., respectively, which is larger than the range previously reported for these minerals. Sulpharsenide compositions can be grouped into three populations, which conform to cobaltian arsenopyrite, cobaltite and gersdorffite. They display highly variable As/S ratios between 0.95:1.00 and 1.29:0.73, consistent with experimental data. Estimates of the formation temperatures, based on the presence of dendritic native bismuth and emplectite, are in the range 100−300°C, similar to different post-Variscan mineralization styles widespread in Central Europe. Comparison of the Co-Ni-Bi vein assemblage with the framework of available paragenetic information and radiometric age data for regional mineralization events indicates an age of mineralization of ~150−160 Ma for the Bieber deposit.

KEYWORDS: Co-Ni-Bi ores, Bieber, Spessart, skutterudite, diarsenides, sulpharsenides.

Introduction

BASE metal deposits related to the Permian Kupferschiefer are widespread in central Europe and have been the subjects of extensive mineralogical-geochemical investigation (e.g. Vaughan *et al.*, 1989; Speczik, 1995). The Kupferschiefer hosts two different types of mineralization: (1) stratabound mineralizations of Cu, Ag, As, Au and PGE, and (2) crosscutting epigenetic vein-type mineralizations of Co, Ni, Bi and As. Most of the recent studies have focused on the stratabound mineralization style, emphasizing the importance of post-depositional processes (diagenetic to epigenetic) for the metal accumulation and re-distribution within the Kupferschiefer deposits (e.g. Sun and Püttmann, 1997). These investigations have focused on ore mineralogy, trace element analysis, stable isotope and organic-geochemical studies (e.g. Bechtel and Püttmann, 1991; Sun and Püttmann, 2000). The epigenetic vein-type Co-Ni-Bi mineralizations have not been studied to the same extent, and only limited mineralogical-geochemical data are available for this mineralization style (e.g. Gerlach, 1992).

The present study reports the results of mineralogical investigations carried out on vein-type Co-Ni-Bi ores of the Bieber deposit, which belongs to a small area of Kupferschiefer-related base metal mineralizations located in the NW part of the Spessart mountains (Fig. 1). The Bieber deposit is the type locality of the rare supergene minerals bieberite, $CoSO_4 \cdot 7\,H_2O$, and rösslerite, $MgH[AsO_4] \cdot 7\,H_2O$; samples originating from the Co-Ni-Bi veins are held by most of the important mineralogical museums throughout Europe (including Museum für Naturkunde, Berlin, Natural History Museum, London, and Ecole des Mines, Paris). The ore assemblages of the Co-Ni-Bi veins are similar to other epigenetic Kupferschiefer-related deposits, e.g. Richelsdorf, Mansfeld and Sangerhausen (Kautzsch, 1953; Rentzsch and Knitzschke, 1968; Tobschall et al., 1986; Gerlach, 1992), but show some distinct features, such as the presence of large amounts of native bismuth and very complex intergrowths of Co-Ni arsenides and sulpharsenides. The major objectives of this investigation are (1) to establish a mineralogical characterization of the Co-Ni-Bi ore assemblages, and (2) to place some constraints on the genetic evolution of the Bieber deposit.

Regional geological setting

The Spessart mountains constitute a part of the Mid-German Crystalline Rise, which belongs to the internal zone of the mid-European Variscan Orogen (Weber, 1995). The crystalline basement can be divided into several SW−NE-striking tectono-metamorphic units, which are: (1) Alzenau formation (biotite and hornblende gneisses, amphibolites); (2) Geiselbach formation (quartzites, mica schists, amphibolites); (3) Mömbris formation (staurolite-garnet-plagioclase gneisses, muscovite-biotite gneisses); (4) Schweinheim formation (mica schists, biotite gneisses); and (5) Elterhof formation (amphibolites, calcsilicate gneisses, marbles, hornblende gneisses). Pervasive deformation and peak metamorphism occurred during the Variscan orogeny at ~320−330 Ma (Weber, 1995). The metasedimentary rocks are crosscut by several lamprophyric dykes (Wrobel, 2000) and intruded by late Permian rhyolitic magmas.

The crystalline basement is unconformably overlain by Permian sedimentary rocks of the Zechstein (Zechstein 1, Werra cycle), which comprises conglomerates, the Kupferschiefer and bituminous dolomites (Fig. 1). The lowermost unit of the Zechstein is composed of component-supported conglomeratic sandstones, 1−2 m thick, which have a predominantly dolomitic cement. These conglomeratic sandstones are overlain by the Kupferschiefer, which represents an intercalation of bituminous argillaceous to silt-rich shales, dolomite-rich siltstones and dolostones. The Kupferschiefer reaches a maximum thickness of 2.2 m (mean of 0.7 m) and is followed by the Zechstein dolomite unit. The
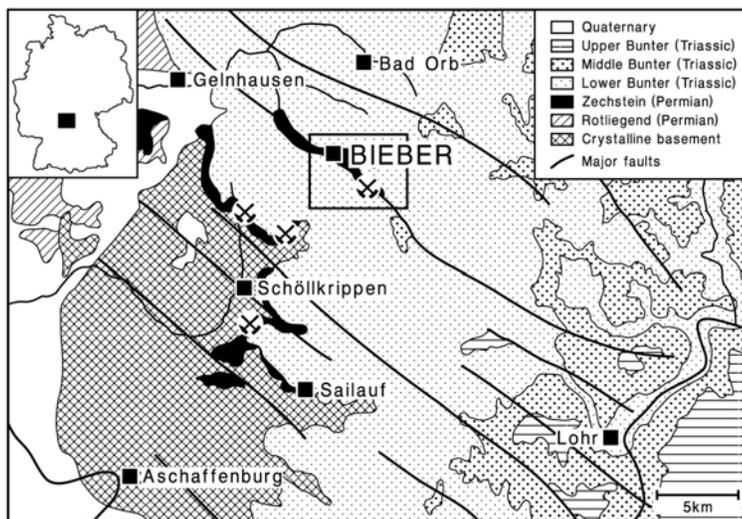

FIG. 1. Geological sketch map of the northern part of the Spessart, showing the locations of the Bieber Co-Ni-Bi deposit as well as of several other Co-Ni and Cu deposits. Redrawn and modified after Matthes and Okrusch (1965).

lowermost part of the Zechstein dolomite is composed of platy bituminous dolostones with mm-thick interlayers of silty dolostones, whereas the middle and upper parts are pure dolostones (Schmitt, 1992, 1993a). The sedimentary rocks of the Zechstein are overlain by the siliciclastic successions of the Lower, Middle and Upper Bunter (Triassic), which represent a complex sequence of sandy shales, sandstones and conglomeratic sandstones.

Both the Variscan crystalline basement and the sedimentary rocks of the post-Variscan cover are crosscut by NW−SE-striking fault systems (Figs 1,2), which were activated as a consequence of the post-Variscan extensional regime in Central Europe (e.g. Ziegler, 1987). These fault systems, which dip 45−80° towards the SW and NE, are frequently mineralized with baryte and quartz (Murawski, 1954; Hofmann, 1979), and carry local enrichments of Bi minerals, which are dominated by emplectite and native bismuth (Schmitt, 1993b). Vein-type Co-Ni-Bi assemblages occur only in close contact with the sedimentary rocks of the Zechstein. A more complex mineralization style has been reported from a structurally similar fault zone exposed in the Lower Permian rhyolite of Sailauf, where Mn ore assemblages (Mn oxides and carbonates)

occur in close association with native arsenic, native bismuth and several accessory minerals (Lorenz, 1991, 1995). Geochronological investigations have demonstrated that the onset of mineralization was at ~180 Ma; hydrothermal activity occurred at several distinct stages and continued until ~100 Ma (Hautmann et al., 1999).

The Bieber Co-Ni-Bi deposit

Mining activities in the Bieber area were first recorded in 1542, when early workings concentrated on stratabound Cu-Pb-Ag mineralizations in the Kupferschiefer. The major mining period, which focused on the cobalt ores of the Co-Ni-Bi vein deposits, was from 1731 to 1869 (Freymann, 1991). Most of the samples held within museums were collected during this period. The Co-Ni-Bi mineralization of the Bieber deposit comprises four distinct vein systems, which are: (1) the Büchelbach Co veins; (2) the Röhrig Co veins; (3) the Lochborn Co veins; and (4) the Bismuth vein (Fig. 2). All vein systems represent mineralized parts of the post-Variscan fault zones, which were still active during ore formation, as demonstrated by brecciation and partial mylonitization of the older ore assemblages. Most of the veins display a NW−SE strike in the range
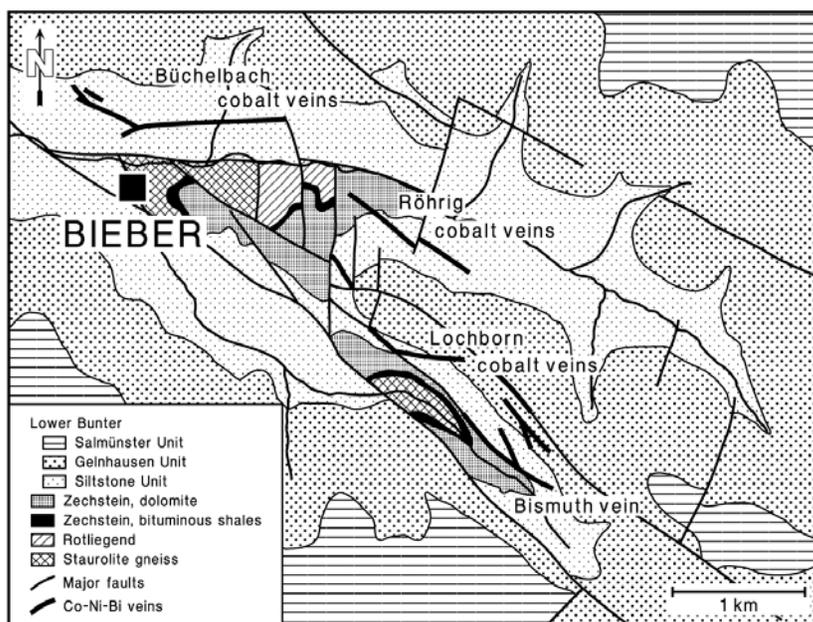

Fig. 2. Detailed geological map of the Bieber Co-Ni-Bi deposit, Spessart, Germany, showing the principal arrangement of the vein systems. Redrawn and modified after Diederich and Laemmlen (1964).

120–150°, and dip 40–70° towards the SW and NE. Only the major vein of the Büchelbach cobalt vein system shows a diverging E–W strike (Fig. 2). The vein dimensions range from a few cm to ~6 m, with mean values in the range 0.15–1.50 m (Freyman, 1991). The mineralized fault zones, which are exposed in the crystalline basement, the Zechstein sediments and the overlying Lower Bunter, are mainly filled with baryte, siderite and strongly-altered wallrock fragments. It is important to note that the occurrence of Co-Ni-Bi ores, which form local concentrations in the veins, is restricted to the crystalline basement and the lowermost part of the Zechstein sediments (Kupferschiefer and lower part of the dolomite unit). Major components of the Co-Ni-Bi ores are skutterudite, niccolite, safflorite, rammelsbergite/pararammelsbergite and native bismuth. Although most of the veins contain native bismuth in close association with the Co-Ni ores, the most important enrichments of native bismuth occur within a particular vein, in the SE part of the deposit (the bismuth vein).

Mineralogy of the Co-Ni-Bi ores

Most of the sample material investigated in this study was obtained from museum collections; additional material was collected from dumps of the Lochborn and Röhrig Co veins. A total of 68 samples was studied by reflected-light micro-

scopy, electron-probe microanalysis and X-ray powder diffraction. Ore mineral assemblages from 16 representative samples are listed in Table 1. The vein-type Co-Ni-Bi ores occur as local enrichments and impregnations in a gangue composed of tabular baryte crystals and massive siderite. Most of the Co-Ni arsenide assemblages are present as complex zoned rosettes, botryoidal masses and idiomorphic crystals, which were subsequently overgrown by siderite. The vein ores were subjected to several stages of tectonic movement along the fault zones, which resulted in extensive fracturing and brecciation of the older assemblages. On the basis of the mineral assemblages and textural relationships, three sequential stages of deposition can be distinguished: (1) the Cu stage; (2) the main Co-Ni-Bi stage; and (3) the late stage (Fig. 3).

The mineralization sequence initiated with the formation of quartz, which is a relatively subordinate gangue mineral. Quartz is present as idiomorphic prismatic crystals, which are commonly enclosed in tabular baryte I. The baryte has been overgrown by the principal ore minerals of the Cu stage, mainly chalcopyrite and tennantite. Chalcopyrite, galena and sphalerite are present as anhedral inclusions within tennantite, which forms both massive aggregates, up to 3–4 cm in size, and idiomorphic crystals. Tennantite close to fault zones has been strongly brecciated. The intensity of the brecciation

TABLE 1. Description of representative samples from the Bieber Co-Ni-Bi deposit.

| Sample	Source/location	Ore assemblage
BIE-2	Aschaffenburg natural history museum	Maucherite, niccolite, native bismuth
BIE-32	Aschaffenburg natural history museum	Cobaltite, cobaltian arsenopyrite, skutterudite, native bismuth
BIE-79	Aschaffenburg natural history museum	Gersdorffite, rammelsbergite, safflorite, skutterudite
BIE-124	University of Straßburg	Emplectite, loellingite, skutterudite, native bismuth
BIE-129	University of Straßburg	Skutterudite, native bismuth
BIE-132b	University of Straßburg	Safflorite, skutterudite, native bismuth
BIE-149	University of Straßburg	Tennantite, chalcopyrite, pyrite, sphalerite, galena
BIE-151a	University of Straßburg	Emplectite, safflorite, skutterudite, native bismuth
BIE-243	University of Straßburg	Niccolite, gersdorffite, safflorite, rammelsbergite, loellingite, native bismuth
BIE-254	Röhrig cobalt vein	Alloclasite, skutterudite
BIE-264	Röhrig cobalt vein	Gersdorffite
BIE-448a	Bieber, not further specified	Skutterudite, native bismuth
BIE-452a	University of Karlsruhe	Tennantite, skutterudite, marcasite, pyrite
BIE-456	University of Stuttgart	Cobaltite, safflorite, loellingite, skutterudite
BIE-457	University of Karlsruhe	Native bismuth, bismuthinite, loellingite, tetrahedrite
BIE-460	University of Karlsruhe	Safflorite, loellingite, skutterudite
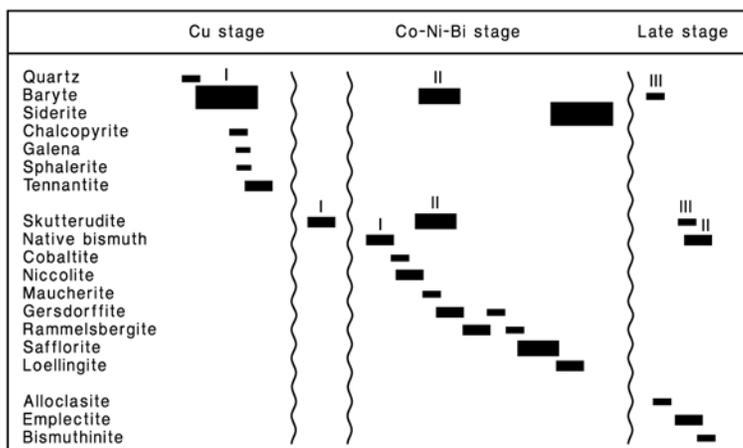
FIG. 3. Paragenetic sequence of the Bieber Co-Ni-Bi mineralisation, as determined through textural observations. The vertical lines indicate brecciation events.

decreases with increasing distance from the faults. Subsequent to the brecciation event, skutterudite I precipitated within the microfractures of the tennantite breccia (Fig. 4a). This skutterudite is composed of numerous very minute (5−20 μm) idiomorphic crystals, which display a significant growth zonation and hopper crystal morphology, indicative of rapid deposition. Skutterudite I is also present as strongly-fractured and brecciated skeletal crystals, which were overgrown and enclosed by later emplectite (Fig. 4b).

In contrast to skutterudite I, the later skutterudite II, which makes up most of the massive Co-Ni-Bi ores, does not show evidence of extensive brecciation. Skutterudite II, which was deposited subsequent to cobaltite and native bismuth I, is present as idiomorphic cubo-octahedral crystals, 0.2−8.5 mm in size (Fig. 4c), anhedral massive aggregates (Fig. 4d), dendritic aggregates (Fig. 4e) and composite idiomorphic crystals which display a significant growth zonation (Fig. 4f). Native bismuth, up to 5 mm in size, is commonly found both as large dendritic aggregates, which are enclosed in skutterudite (Fig. 4d) and emplectite (Fig. 4b). Very commonly, the dendritic bismuth is surrounded by radial microfractures, a texture initially described by Ramdohr (1981). Anhedral grains of native bismuth are rarely found as inclusions within cobaltite and cobaltian arsenoyprite, which both display euhedral to subhedral grain shapes; cobaltite and cobaltian arsenopyrite were subsequently overgrown and enclosed by massive skutterudite (Fig. 4d). The larger dendritic aggregates of native bismuth are surrounded by a layer of skutterudite, which shows idiomorphic terminations. Skutterudite hosting dendritic native bismuth is enclosed by massive baryte II or has idiomorphically grown upon this baryte, which indicates that deposition of skutterudite II was approximately contemporaneous with baryte II.

Complex diarsenide/sulpharsenide rosettes, composed of rammelsbergite/pararammelsbergite, gersdorffite, safflorite and loellingite, have formed subsequent to skutterudite. Two distinct textural types can be distinguished, which are: (1) rammelsbergite/pararammelsbergite-rich assemblages surrounding niccolite; and (2) safflorite-rich assemblages surrounding skutterudite. Niccolite, which is present as anhedral grains, and rarely associated with massive maucherite (Fig. 5a), constitutes the core of the Ni-rich rosettes. Niccolite contains anhedral and dendritic inclusions of native bismuth, but no inclusions of skutterudite, indicating more or less contemporaneous formation of niccolite and skutterudite. The Ni-rich diarsenide/sulpharsenide rosettes are characterized by a complex growth zoning. Niccolite has been overgrown by alternating bands of gersdorffite and rammelsbergite/pararammelsbergite, which were followed by later idiomorphic safflorite and loellingite (Fig. 5b). The sequence of gersdorffite and rammelsbergite/pararammelsbergite is found to be repeated twice, which indicates oscillating precipitation conditions. It is important to note that the presence of both rammelsbergite and pararammelsbergite (Fleet, 1972) has been confirmed by X-ray
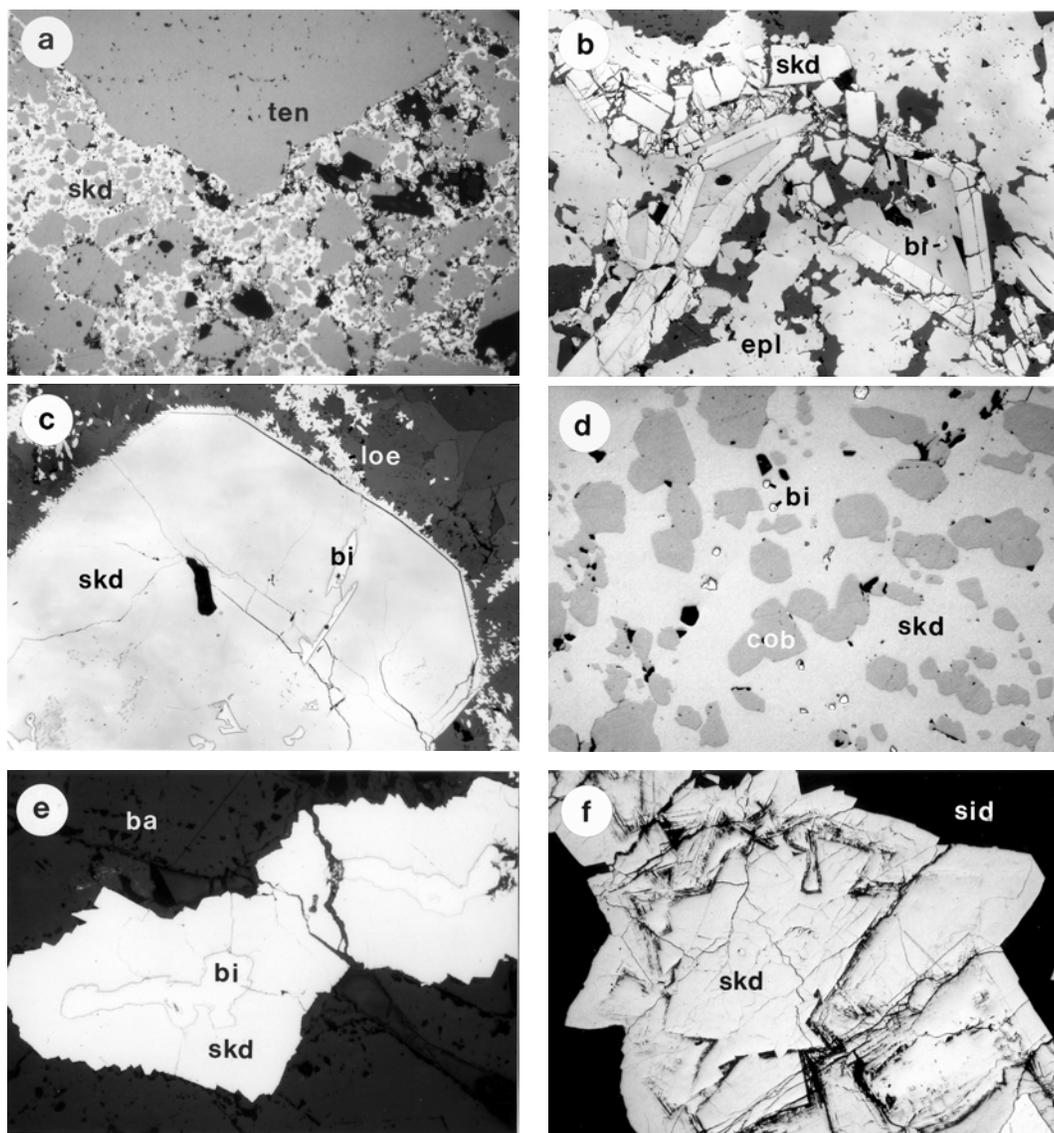
389

FIG. 4. Photomicrographs in reflected light showing various representative textures of the Bieber Co-Ni-Bi ores. (*a*) Brecciated tennantite (ten) close to a fault zone has been infilled by skutterudite I (skd). Sample BIE-452a. Width of field: 1.15 mm. (*b*) Skutterudite I (skd) has been strongly brecciated. Subsequently, native bismuth I (bi) has precipitated as anhedral grains. Both skutterudite and native bismuth have been overgrown by prismatic emplectite (epl). Sample BIE-151a. Width of field: 1.39 mm. (*c*) Native bismuth I (bi), present as dendritic aggregates, has been overgrown and enclosed by an idiomorphic crystal of skutterudite II (skd). In contrast to skutterudite I, skutterudite II does not show extensive brecciation. Idiomorphic crystals of loellingite (loe) have grown upon the crystal faces of skutterudite. Sample BIE-124. Width of field: 2.65 mm. (*d*) Subhedral crystals of cobaltite (cob) and anhedral grains of native bismuth (bi) are both present as inclusions within massive skutterudite II (skd). Sample BIE-32. Width of field: 500 μm. (*e*) Skutterudite II (skd), hosted by baryte (ba), has overgrown and enclosed dendritic native bismuth I (bi). Sample BIE-448a. Width of field: 1.0 mm. (*f*) Skutterudite II (skd) showing complex growth zoning, has been enclosed by later siderite (sid). Sample BIE-129. Width of field: 2.35 mm.
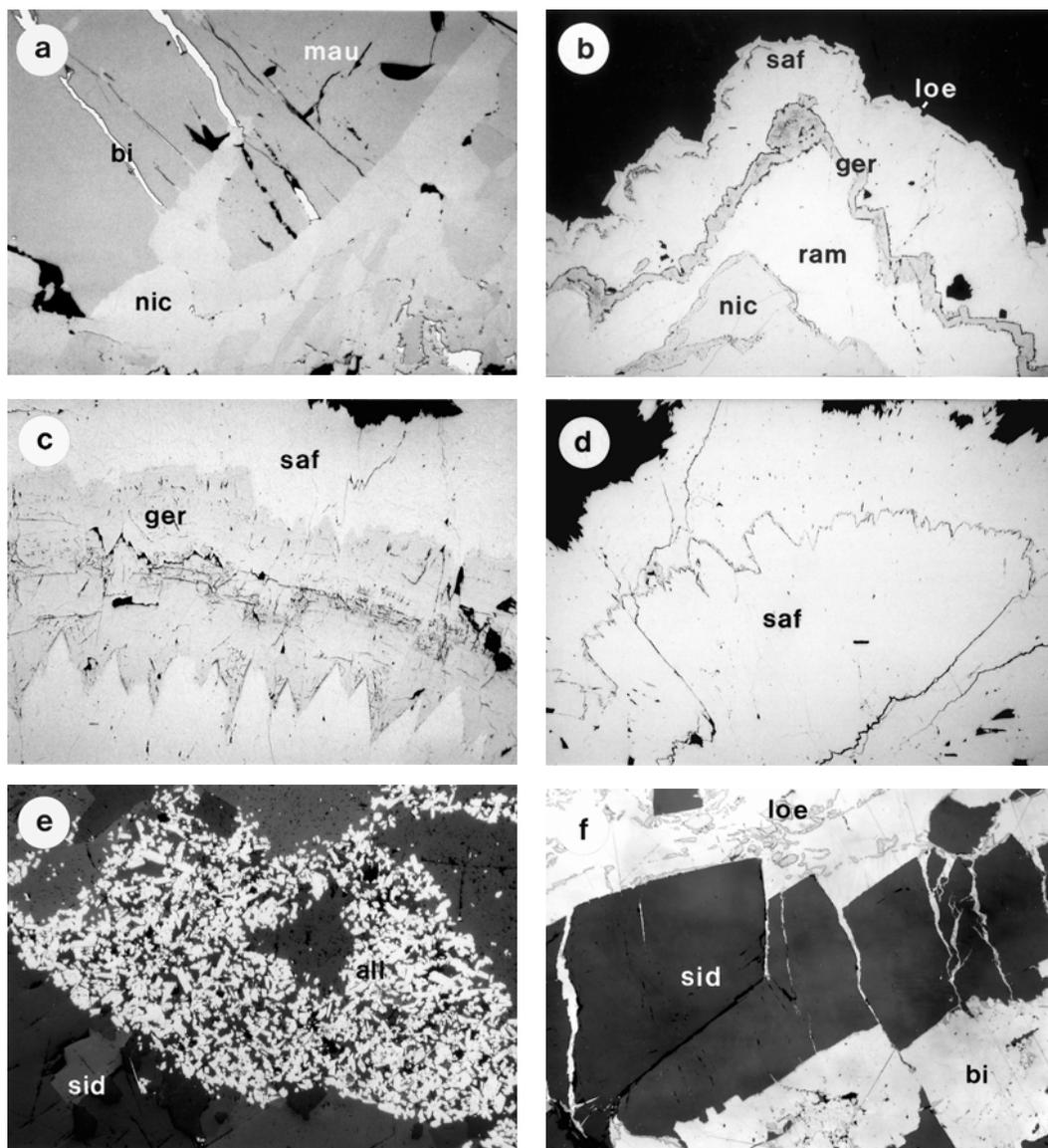
Fig. 5. Photomicrographs in reflected light showing various representative textures of the Bieber Co-Ni-Bi ores. (*a*) Niccolite (nic) has been overgrown by maucherite (mau). Subsequently, microfractures within maucherite were filled by native bismuth II (bi). Sample BIE-2. Width of field: 560 μm. (*b*) A typical niccolite-rich rosette, showing a complex oscillatory growth zoning. Niccolite (nic) has been overgrown by alternating bands of gersdorffite (ger) and rammelsbergite/pararammelsbergite (ram), which were followed by late safflorite (saf) and idiomorphic crystals of loellingite (loe). Sample BIE-243. Width of field: 1.75 mm. (*c*) Detail of a gersdorffite band in a Co-rich rosette, showing idiomorphic terminations of both safflorite (saf) and gersdorffite (ger). Sample BIE-456. Width of field: 1.07 mm. (*d*) Marginal zone of a Co-rich rosette, which encloses a core of skutterudite. The diarsenide rosette is composed of safflorite (saf), which has a highly variable composition. Sample BIE-132b. Width of field: 3.0 mm. (*e*) Siderite (sid) has been partially replaced by alloclasite (all). Sample BIE-254. Width of field: 2.20 mm. (*f*) Fractures in siderite (sid) have been infilled by native bismuth II (bi). The native bismuth encloses aggregates of loellingite (loe) crystals. Sample BIE-457. Width of field: 1.50 mm.

powder diffraction in several niccolite-rich samples, but it is very difficult to distinguish between them by reflected-light microscopy and electron-probe microanalysis. Therefore, the term rammelsbergite/pararammelsbergite is used for simplicity, referring to both minerals. The Co-rich rosettes, which most commonly enclose a core of skutterudite, are found to be composed of safflorite and gersdorffite. Both safflorite and gersdorffite show idiomorphic terminations (Fig. 5c), indicating relatively slow deposition of both minerals within open fracture zones. The marginal zones of the Co-rich rosettes are characterized by several individual growth zones of safflorite (Fig. 5d). Both textural types of diarsenide/sulpharsenide rosettes are overgrown by massive siderite, which has filled most of the remaining open space within the Co-Ni-Bi veins.

Portions of the massive siderite show extensive brecciation and infilling by the late stage assemblages. In places, the fractured siderite has been replaced by alloclasite, which is present as accumulations of rhomb-shaped idiomorphic crystals (Fig. 5e). Alloclasite is closely associated with a late generation of skutterudite, which forms isolated cube-shaped crystals enclosing idiomorphic alloclasite. Local enrichments of native bismuth are related to extensively brecciated siderite. Fractures and micro-faults in siderite have been infilled by massive native bismuth II, which hosts inclusions of rhomb-shaped idiomorphic crystals of loellingite and anhedral grains of bismuthinite (Fig. 5f). Inclusions of loellingite are also present within the siderite, indicating loellingite formation during precipitation and subsequent brecciation of the siderite. Emplectite is apparently a late mineral in the sequence of deposition, because aggregates composed of acicular to prismatic crystals of emplectite are commonly found in vugs within siderite. Massive emplectite hosts inclusions of corroded siderite, native bismuth and brecciated skutterudite (Fig. 4b). The massive anhedral native bismuth II is rarely crosscut by late microfractures, which have been partially filled by tetrahedrite.

Mineral chemistry

The chemical composition of the mineral phases was determined by wavelength-dispersive electron-probe microanalysis using the CAMECA SX-50 instrument in Würzburg. Operating conditions were 15 kV at a beam current of 15 nA, a beam size of $1-2$ µm and counting times of 20 s on TAP/PET and 30 s on LiF. Standards and radiations used were as follows: Se (Lα), Te (Lα), Cd (Lα), Ag (Lα), Bi (Mα), Au (Mα), Cu (Kα), Co (Kα) and Ni (Kα), GaAs (As-Lα), FeS_2 (Fe-Kα, S-Kα), ZnS (Zn-Kα), Sb_2S_3 (Sb-Lα), PbS (Pb-Mα), HgS (Hg-Mα), SnO_2 (Sn-Lα) and $MnTiO_3$ (Mn-Kα). Under the current analytical conditions, the detection limit for these elements is in the range of 0.1 wt.%; the analytical precision is ~1% for all major elements. The total number of analyses performed for each mineral or mineral group is given in brackets in the following paragraphs.

Ni arsenides

The compositions of the two Ni arsenide minerals, niccolite ($n = 22$) and maucherite ($n = 24$), are characterized by relatively limited variability. Niccolite and maucherite display Co incorporation in the range $0.28-0.62$ wt.% and $0.65-1.19$ wt.%, respectively, whereas the concentration of Fe is generally <0.1 wt.% (Table 2). Minor substitution of As by S is only detectable in maucherite ($0.20-0.25$ wt.%), whereas the S concentrations in niccolite are below the detection limit.

Skutterudite

Skutterudite ($n = 159$) displays a broad range of compositional variation. The most important feature is a substantial substitution of Co by Ni and Fe, which is in the range $0.11-14.39$ wt.% and $0.46-7.97$ wt.%, respectively (Table 3). The skutterudite compositions detected in the Bieber Co-Ni-Bi ores include both skutterudite and Ni-skutterudite, which confirms the results of X-ray powder diffraction analyses. Refinement of the XRD data indicates that two types of skutterudite are present, which have cell parameters of $8.172-8.225$ Å and $8.259-8.265$ Å. These conform to the values of 8.204 and 8.303 Å listed for skutterudite and Ni-skutterudite in the JCPDS powder diffraction data file. On the basis of their compositions in Fe-Co-Ni space, two distinct types of skutterudite can be distinguished. Most of the analytical data fall within a large field corresponding to the known field of skutterudite solid-solution (Roseboom, 1962; Klemm, 1965a; Rosner, 1970), whereas relatively few analyses define a separate group, characterized by elevated Fe and Ni concentrations (Fig. 6a). Although

TABLE 2. Representative electron microprobe analyses of niccolite and maucherite.

Sample	BIE-2 8 nic	BIE-2 17 nic	BIE-2 41 nic	BIE-2 22 mau	BIE-2 27 mau	BIE-2 50 mau
Wt.%						
Co	0.62	0.34	0.28	0.80	1.19	0.65
Ni	42.26	43.31	43.77	50.61	50.61	51.25
As	56.50	55.89	55.96	49.14	48.92	48.43
S	<0.1	<0.1	<0.1	0.20	0.23	0.25
Se	0.26	0.29	0.34	0.35	<0.1	0.28
Total	99.64	99.83	100.35	101.10	100.95	100.86
Formulae						
Co	0.01	0.01	0.01	0.17	0.25	0.14
Ni	0.98	0.99	0.99	10.82	10.74	10.86
As	1.03	1.00	1.00	8.23	8.13	8.04
S	0	0	0	0.08	0.09	0.10

most of the crystals and aggregates of skutterudite display a significant growth zonation, it is not possible to correlate the observed compositional trends with a distinct zonation pattern. The compositional variations between different aggregates and grains are similar to those between individual growth zones. In addition to the variation of skutterudite in Fe-Co-Ni space, a significant substitution of As by S in the range $0.15-5.43$ wt.%, corresponding to $0.01-0.44$ atoms per formula unit (a.p.f.u.), has been detected (Fig. 7a). The As concentrations are negatively correlated with the S concentrations over the entire compositional range ($R^2 = 0.86$).

Interestingly, the Fe- and Ni-rich skutterudites defining a separate group in Fe-Co-Ni space display the lowest S concentrations. The Me:(As+S) ratios of the skutterudites range between 1:2.90 and 1:3.03 and are very close to the ideal stoichiometry. It is noted that the skutterudite compositions displaying elevated levels of S substitution tend to be closer to the ideal Me:(As+S) value. The extent of deviation of skutterudite from ideal stoichiometry has been the subject of much discussion. Synthetic skutterudite corresponding to the Co end-member was found to be almost stoichiometric with Me:As ratios in the range 1:2.95 to 1:2.97 (Roseboom, 1962).
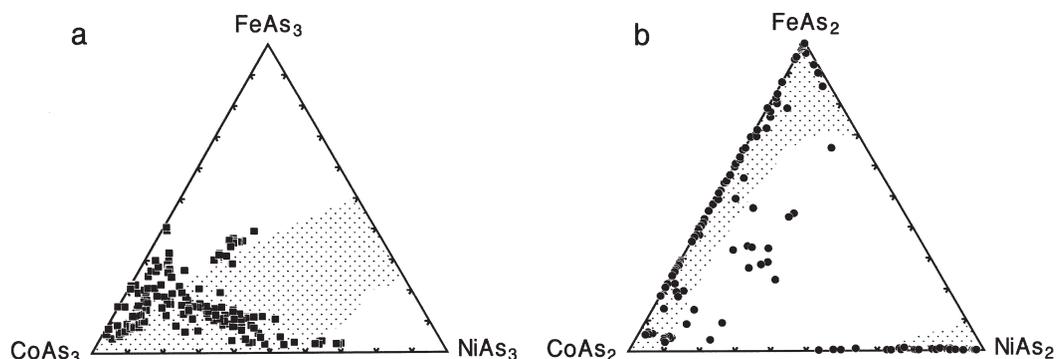
FIG. 6. Compositional representations (mol.%) of skutterudites and diarsenides. Both diagrams show a summary of data from all samples analysed. (a) Skutterudites in the system FeAs$_3$-CoAs$_3$-NiAs$_3$. The shaded area indicates the maximum field of solid-solution at 800°C (Roseboom, 1962), which conforms to the known range of natural skutterudite compositions (Rosner, 1970). (b) Diarsenides in the system FeAs$_2$-CoAs$_2$-NiAs$_2$. The shaded area shows the field of natural diarsenides (Roseboom, 1963).

FIG. 7. Variation of As and S a.p.f.u. in (*a*) skutterudites, and (*b*) diarsenides from the Bieber deposit.

Systematic microprobe studies of natural skutter-
udite by Klemm (1965*a*) found a compositional
variation between 1:1.9 and 1:3.3, which could
not be confirmed in subsequent studies (e.g.
Rosner, 1970; Petruk *et al*., 1971; Ixer *et al*.,
1979; Zakrzewski *et al*., 1980; Oen *et al*., 1984).
The non-stoichiometric skutterudite analyses
reported in the literature may relate to very fine-
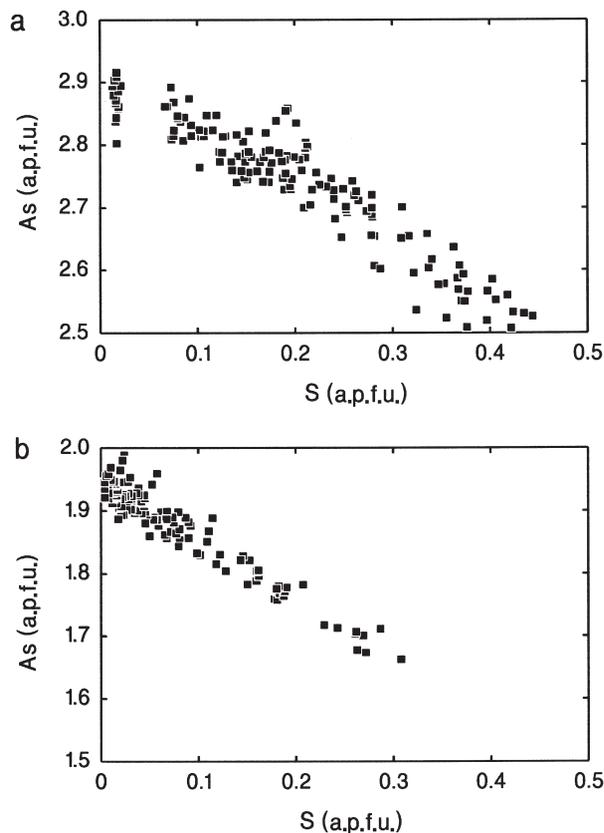grained intergrowths with different diarsenides or
the presence of significant amounts of S
substituting for As, comparable to skutterudite
of the Bieber deposit.

Diarsenides

The different diarsenide minerals (*n* = 133),
comprising safflorite, loellingite and rammelsber-
gite/pararammelsbergite, are characterized by
extensive compositional variability in Fe-Co-Ni
space (Fig. 6*b*). Most of the analytical data plot
along the join connecting safflorite and loellingite

(Table 4, Table 5). In contrast, evidence of solid-
solution between safflorite and rammelsbergite/
pararammelsbergite tends to be more restricted.
The incorporation of Co into rammelsbergite/
pararammelsbergite is in the range
0.64−13.78 wt.% (corresponding to
0.02−0.46 a.p.f.u.), whereas Ni substitution in
safflorite is limited to a maximum of 9.09 wt.%
(corresponding to 0.23 a.p.f.u.). Most of the
analytical data plot within the known field of
diarsenide compositions in Fe-Co-Ni space
(Roseboom, 1963; Radcliffe and Berry, 1968),
whereas a limited number of Fe- and Ni-rich
safflorites have compositions outside this estab-
lished field (Fig. 6*b*). The diarsenides display a
substitution of As by S in the range 0.11−
5.13 wt.%, corresponding to 0.01−0.31 a.p.f.u.
(Fig. 7*b*); the As concentrations are negatively
correlated with the S concentrations (R^2 = 0.92).
It is noted that the relative proportion of S
substituting for As, expressed as S/(As+S) is very

Table 3. Representative electron microprobe analyses of skutterudite.

Sample	BIE-32 14	BIE-79 27	BIE-124 31	BIE-129 28	BIE-132b 39	BIE-151a 27	BIE-254 3	BIE-448a 4	BIE-452a 55	BIE-456 50
Wt.%										
Cu	<0.1	<0.1	0.33	<0.1	<0.1	0.21	<0.1	0.21	0.19	<0.1
Fe	1.76	2.07	7.97	0.46	0.54	5.35	3.41	4.25	1.93	1.29
Co	17.88	12.31	7.41	9.35	6.28	12.85	17.08	17.10	19.05	20.69
Ni	1.54	6.87	5.63	11.03	14.39	2.68	1.72	0.11	1.13	0.25
As	78.55	76.78	78.14	75.31	77.62	75.86	72.81	72.65	72.29	71.78
S	0.15	1.24	0.90	2.29	0.88	2.02	4.52	4.40	5.43	5.28
Se	0.30	0.51	0.34	0.37	0.39	0.57	0.24	0.22	0.24	0.49
Total	100.18	99.78	100.72	98.81	100.10	99.54	99.78	98.94	100.26	99.78
Formulae (calculated to 1 metal)										
Fe	0.09	0.10	0.39	0.02	0.03	0.26	0.16	0.20	0.09	0.06
Co	0.84	0.57	0.34	0.45	0.30	0.60	0.76	0.78	0.85	0.93
Ni	0.07	0.32	0.26	0.53	0.68	0.13	0.08	0.00	0.05	0.01
As	2.90	2.81	2.82	2.83	2.87	2.79	2.55	2.61	2.53	2.53
S	0.01	0.11	0.08	0.20	0.08	0.17	0.37	0.37	0.44	0.43

TABLE 4. Representative electron microprobe analyses of safflorite.

Sample	BIE-79 14	BIE-79 36	BIE-132b 1	BIE-132b 17	BIE-151a 22	BIE-243 10	BIE-243 13	BIE-456 31	BIE-460 35	BIE-460 36
Wt.%										
Cu	0.12	0.19	0.48	0.25	0.49	<0.1	<0.1	<0.1	<0.1	<0.1
Fe	2.47	2.46	10.99	4.96	9.01	0.95	1.67	12.91	6.72	9.33
Co	23.41	19.75	17.30	24.07	15.76	25.59	26.76	15.03	14.45	12.99
Ni	3.46	6.18	<0.1	<0.1	3.78	2.34	0.69	<0.1	9.09	6.68
As	66.56	68.99	71.36	67.81	68.55	70.95	70.24	70.37	64.79	68.66
S	3.02	1.36	0.18	2.60	2.34	0.35	1.17	0.43	5.13	2.46
Se	0.22	0.43	0.21	0.39	0.29	0.48	0.31	0.51	0.20	0.13
Total	99.26	99.36	100.52	100.08	100.22	100.66	100.84	99.25	100.38	100.25
Formulae (calculated to 1 metal)										
Fe	0.09	0.09	0.39	0.18	0.32	0.03	0.06	0.47	0.23	0.33
Co	0.79	0.69	0.59	0.81	0.53	0.88	0.91	0.52	0.47	0.44
Ni	0.12	0.22	0.00	0.00	0.13	0.08	0.02	0.00	0.30	0.23
As	1.76	1.89	1.91	1.80	1.83	1.92	1.89	1.93	1.66	1.82
S	0.19	0.09	0.01	0.16	0.15	0.02	0.07	0.03	0.31	0.15

Table 5. Representative electron microprobe analyses of rammelsbergite and loellingite.

Sample	BIE-79 6 ram	BIE-79 10 ram	BIE-243 20 ram	BIE-243 25 ram	BIE-243 26 ram	BIE-124 30 loe	BIE-243 3 loe	BIE-243 5 loe	BIE-457 27 loe	BIE-460 14 loe
Wt.%										
Cu	<0.1	<0.1	<0.1	<0.1	<0.1	0.16	<0.1	<0.1	<0.1	<0.1
Fe	0.14	0.19	<0.1	<0.1	<0.1	28.34	24.83	23.00	25.43	21.30
Co	4.24	10.82	13.78	0.64	6.65	<0.1	0.37	0.60	1.35	6.02
Ni	24.85	19.16	15.86	28.39	21.75	<0.1	2.53	3.43	<0.1	0.41
As	66.62	64.51	71.25	71.72	71.39	67.97	71.51	71.79	71.91	71.55
S	3.31	4.48	0.29	0.11	0.16	3.12	0.71	0.38	0.88	0.20
Se	0.29	0.24	0.51	0.32	0.41	0.40	0.37	0.32	0.12	0.41
Total	99.45	99.40	101.69	101.18	100.36	99.99	100.32	99.52	99.69	99.89
Formulae (calculated to 1 metal)										
Fe	0.01	0.01	0.00	0.00	0.00	1.00	0.90	0.85	0.95	0.78
Co	0.14	0.36	0.46	0.02	0.23	0.00	0.01	0.02	0.05	0.21
Ni	0.85	0.63	0.54	0.98	0.77	0.00	0.09	0.12	0.00	0.01
As	1.78	1.67	1.89	1.93	1.97	1.78	1.92	1.99	1.96	1.95
S	0.21	0.27	0.02	0.01	0.01	0.19	0.04	0.02	0.06	0.01

similar for both the diarsenides (0.16) and the safflorites (0.15). Most of the safflorite making up the marginal zones of Co-rich diarsenide/sulpharsenide rosettes displays a significant compositional zonation, which is characterized by alternating Fe-rich and Fe-poor bands (Fig. 9). The Me:(As+S) ratios of the diarsenides range between 1:1.91 and 1:2.02, which is very close to the stoichiometric value.

Sulpharsenides

The different sulpharsenide minerals ($n = 117$) present in the Co-Ni-Bi ores can be grouped into three different populations, based on their compositional trends in Fe-Co-Ni space. Two of these compositional populations, which correspond to cobaltian arsenopyrite and cobaltite, are found exclusively as inclusions in massive skutterudite in sample BIE-32 (Table 6, Fig. 8a). The textural and compositional classification of these two distinct sulpharsenide phases has been confirmed by X-ray powder diffraction analyses. Cobaltian arsenopyrite displays a relatively limited Co substitution (Fig. 8a), which is in the range 5.19−11.23 wt.%, corresponding to 0.15−0.32 a.p.f.u.; the amount of Ni incorporation is insignificant and ranges between 0.46 and 1.52 wt.%. Cobaltite, present in the same sample, is characterized by extended substitution by both Fe and Ni (Fig. 8a) in the range 2.19−8.04 wt.% and 1.07−12.32 wt.%, respectively (corresponding to 0.06−0.24 and 0.03−0.35 a.p.f.u.). The Ni concentrations are positively correlated with the Fe concentrations over the entire compositional range ($R^2 = 0.97$),

indicating that both Fe and Ni substitute for Co in a fixed ratio. A similar solid-solution trend between cobaltite and Co- and Fe-rich gersdorffite has been reported from the Tunaberg skarn deposit, Sweden (Dobbe and Oen, 1994). The sulpharsenides from all other samples investigated are located on a trend connecting cobaltite with gersdorffite (Fig. 8b); the detected compositions range between $Co_{0.92}Ni_{0.01}Fe_{0.07}As_{1.08}S_{0.90}$ and $Co_{0.10}Ni_{0.88}Fe_{0.02}As_{1.14}S_{0.86}$ (Table 7). This compositional trend includes cobaltite, alloclasite and gersdorffite, as shown by X-ray diffraction analyses. The different sulpharsenide minerals show highly variable As/S ratios between 0.95:1.00 and 1.29:0.73, which is consistent with the experimentally-determined compositional range (Klemm, 1965b; Bayliss, 1969).

Tennantite and tetrahedrite

Tennantite ($n = 33$), which is the dominant fahlore mineral in the Bieber Co-Ni-Bi ores, has a composition close to the As end-member, with As/(As+Sb) ratios in the range 0.77−0.98 (Table 8, Fig. 10). The Zn/(Zn+Fe) ratios are in the range 0.19−0.38, and are only very weakly correlated with the As/(As+Sb) ratios ($R^2 = 0.23$). The Ag concentrations are relatively low, in the range 0.16−0.34 wt.%, whereas most analytical data display a significant substitution of As by Bi in the range 0.24−2.55 wt.%. The tennantite compositions correspond well with analytical data reported for tennantite from stratabound mineralizations in different types of Zechstein sediments in the Spessart (Schmitt, 1993a). Tetrahedrite ($n = 6$), present as infilling of late
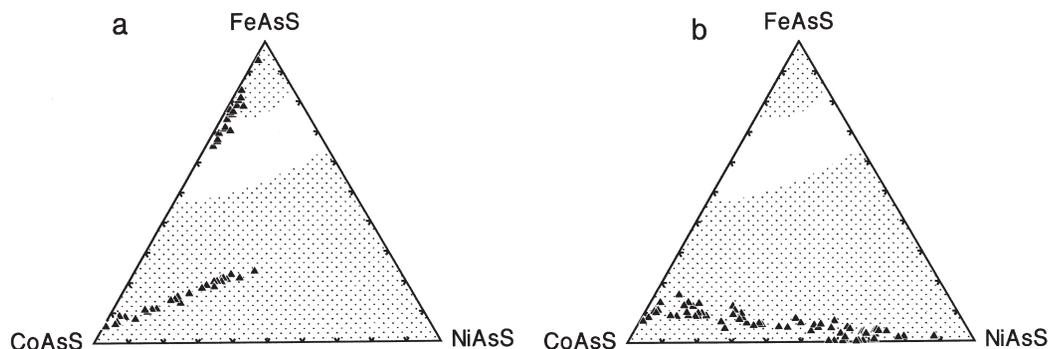

FIG. 8. Compositional representations (mol.%) of sulpharsenides in the system FeAsS-CoAsS-NiAsS. (*a*) Cobaltite and cobaltian arsenopyrite, sample BIE-32. (*b*) Cobaltite, alloclasite and gersdorffite, samples BIE-79, BIE-243, BIE-254, BIE-264 and BIE-456. The shaded area indicates the maximum field of solid-solution at 650°C after Klemm (1965).

TABLE 6. Representative electron microprobe analyses of cobaltian arsenopyrite and cobaltite.

| Sample	BIE-32 8 asp	BIE-32 9 asp	BIE-32 20 asp	BIE-32 29 asp	BIE-32 49 asp	BIE-32 1 cob	BIE-32 4 cob	BIE-32 15 cob	BIE-32 62 cob	BIE-32 65 cob
Wt.%										
Cu	<0.1	<0.1	0.14	<0.1	<0.1	<0.1	<0.1	<0.1	<0.1	<0.1
Fe	22.49	21.41	26.26	27.86	26.41	2.75	4.90	2.19	6.37	8.04
Co	10.87	11.23	6.03	5.19	6.12	30.65	24.75	33.31	20.22	14.93
Ni	0.90	0.70	1.52	0.46	0.65	2.85	5.72	1.07	9.16	12.32
As	49.74	49.74	49.33	48.27	47.82	44.59	45.12	44.43	45.92	46.60
S	16.31	16.88	16.85	17.44	17.94	19.81	19.20	19.74	18.78	18.69
Se	0.27	0.21	0.24	0.18	0.22	0.16	0.25	0.21	0.17	0.15
Total	100.58	100.17	100.37	99.40	99.16	100.81	99.94	100.95	100.62	100.73
Formulae (calculated to 1 metal)										
Fe	0.67	0.65	0.78	0.84	0.80	0.08	0.14	0.06	0.19	0.24
Co	0.31	0.32	0.17	0.15	0.18	0.84	0.69	0.91	0.56	0.42
Ni	0.03	0.02	0.04	0.01	0.02	0.08	0.16	0.03	0.25	0.35
As	1.10	1.13	1.09	1.08	1.09	0.96	0.99	0.95	1.00	1.02
S	0.84	0.90	0.87	0.91	0.95	1.00	0.99	0.99	0.95	0.96
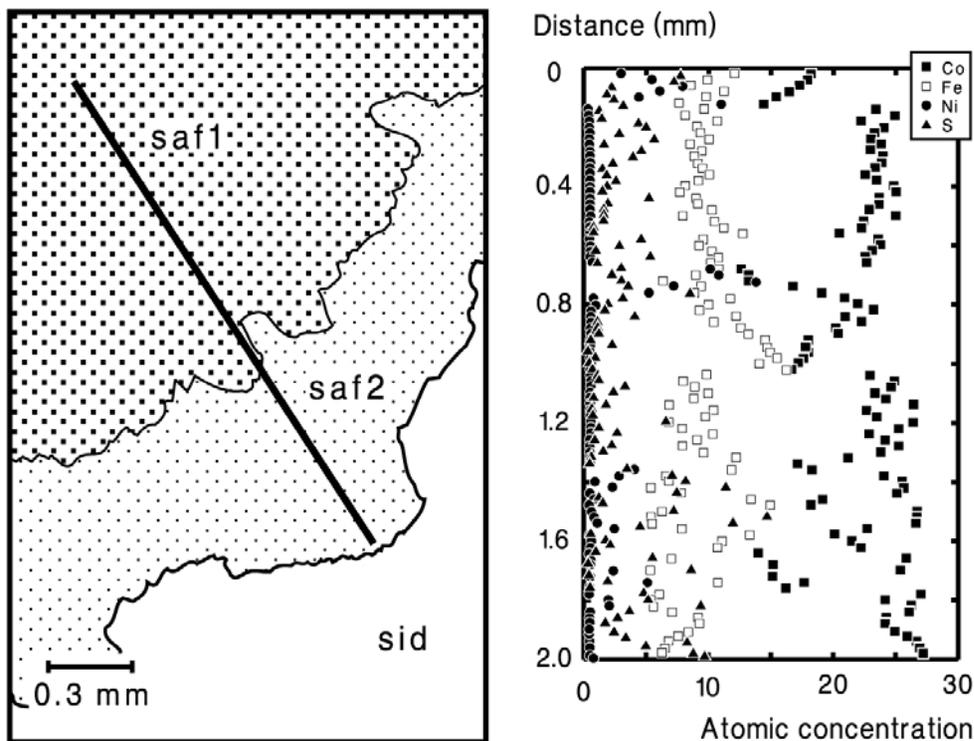
FIG. 9. Schematic section through a complex zoned Co-Ni diarsenide rosette, showing the compositional variation along the traverse. Sample BIE-132b.

microfractures, is characterized by relatively low As concentrations in the range 0.99−2.27 wt.% and the absence of Ag (Table 8). The Zn/(Zn+Fe) ratios vary between 0.65 and 0.96 (Fig. 10).
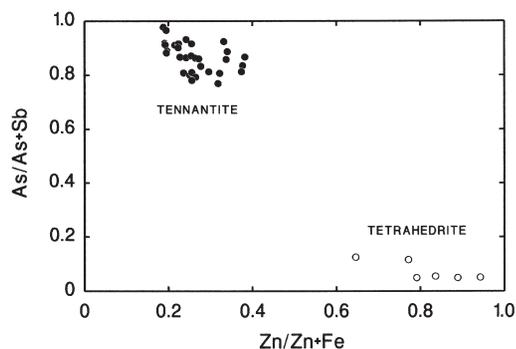

FIG. 10. Compositional representations of tennantite and tetrahedrite, expressed as a plot of As/(As+Sb) vs. Zn/(Zn+Fe).

Bi minerals

The composition of native bismuth ($n = 10$) of the different textural types (anhedral grains, dendritic aggregates, massive enrichments) conforms to the pure element, with only very minor concentrations of Cu detectable. Antimony, which is a common substituent in native bismuth, was not detectable by the electron microprobe (Table 9). Emplectite ($n = 15$) and bismuthinite ($n = 5$) have compositions close to stoichiometry; substitution of Bi by Sb (0.18−0.56 wt.%) in emplectite appears to be insignificant.

Discussion and conclusions

Temperatures of ore formation

Comparison of the sulphide-arsenide assemblages with available experimental data on phase relations enable constraints to be placed on the formation conditions and the genetic evolution of the Bieber ores. Experimental studies have demonstrated that dendritic Bi, texturally compar-

TABLE 7. Representative electron microprobe analyses of cobaltite, alloclasite and gersdorffite.

Sample	BIE-456 8 cob	BIE-456 37 cob	BIE-254 17 all	BIE-254 30 all	BIE-79 1 ger	BIE-243 31 ger	BIE-243 36 ger	BIE-264 5 ger	BIE-264 15 ger	BIE-264 16 ger
Wt.%										
Cu	<0.1	0.17	<0.1	<0.1	<0.1	<0.1	<0.1	<0.1	<0.1	<0.1
Fe	2.43	3.73	1.71	2.98	0.53	<0.1	0.13	0.61	1.91	1.04
Co	31.99	30.58	18.39	26.63	3.64	14.59	13.20	6.57	21.08	10.09
Ni	0.12	1.16	15.67	5.65	29.84	20.02	21.36	26.80	11.59	21.64
As	47.80	46.42	45.76	46.21	49.56	48.72	49.24	50.20	48.59	53.89
S	17.04	18.52	18.88	18.44	15.94	16.49	16.31	15.97	16.91	13.07
Se	0.17	0.22	0.17	0.18	0.24	0.21	0.19	0.29	0.29	0.19
Total	99.55	100.80	100.58	100.09	99.75	100.03	100.43	100.44	100.37	99.92
Formulae (calculated to 1 metal)										
Fe	0.07	0.11	0.05	0.09	0.02	0.00	0.00	0.02	0.06	0.03
Co	0.92	0.85	0.51	0.75	0.10	0.42	0.38	0.19	0.61	0.31
Ni	0.01	0.03	0.44	0.16	0.88	0.58	0.62	0.79	0.33	0.66
As	1.08	1.02	1.00	1.02	1.14	1.10	1.11	1.16	1.10	1.29
S	0.90	0.95	0.96	0.95	0.86	0.87	0.86	0.86	0.89	0.73

TABLE 8. Representative electron microprobe analyses of tennantite and tetrahedrite.

Sample	BIE-149 5 ten	BIE-149 10 ten	BIE-149 16 ten	BIE-149 23 ten	BIE-452a 10 ten	BIE-452a 13 ten	BIE-452a 14 ten	BIE-452a 45 ten	BIE-457 3 tet	BIE-457 5 tet
Wt.%										
Cu	41.84	43.11	43.01	42.70	41.30	42.27	42.01	41.79	39.58	39.42
Ag	0.21	<0.1	0.23	0.16	0.34	0.21	0.30	0.24	<0.1	<0.1
Fe	4.96	5.68	5.71	5.59	4.65	5.27	4.96	4.33	0.97	1.95
Zn	1.95	1.54	1.62	1.59	2.55	2.11	2.17	3.15	5.80	4.19
Hg	0.65	<0.1	0.27	0.15	0.16	0.17	0.15	<0.1	<0.1	<0.1
As	15.76	20.18	19.25	18.19	14.85	16.64	15.88	16.93	0.99	2.27
Sb	6.38	0.73	1.13	3.67	7.16	4.00	4.21	4.25	27.63	25.56
Bi	0.43	0.24	0.24	<0.1	0.64	1.42	2.55	0.65	0.18	0.32
S	27.67	28.01	27.92	28.09	27.03	27.63	27.19	27.54	25.02	25.02
Se	<0.1	<0.1	0.13	<0.1	<0.1	0.11	<0.1	<0.1	<0.1	0.12
Total	99.85	99.49	99.51	100.14	98.68	99.83	99.42	98.88	100.17	98.85
Formulae (calculated to 16 cations)										
Cu	10.04	10.04	10.06	10.02	10.03	10.07	10.11	10.01	10.23	10.31
Ag	0.03	0.00	0.03	0.02	0.05	0.03	0.04	0.03	0.00	0.00
Fe	1.35	1.51	1.52	1.49	1.29	1.43	1.36	1.18	0.28	0.58
Zn	0.46	0.35	0.37	0.36	0.60	0.49	0.51	0.73	1.46	1.07
As	3.21	3.99	3.82	3.62	3.06	3.36	3.24	3.44	0.22	0.50
Sb	0.80	0.09	0.14	0.45	0.91	0.50	0.53	0.53	3.73	3.49
Bi	0.03	0.02	0.02	0.00	0.05	0.10	0.19	0.05	0.01	0.03
S	13.16	12.93	12.94	13.07	13.01	13.04	12.97	13.08	12.82	12.97

TABLE 9. Representative electron microprobe analyses of emplectite and native bismuth.

Sample	BIE-124 5 epl	BIE-151a 10 epl	BIE-124 8 bi	BIE-448a 15 bi	BIE-129 14 bi	BIE-129 34 bi
Wt.%						
Cu	19.48	19.21	0.14	<0.1	0.13	<0.1
Sb	0.18	0.56	<0.1	<0.1	<0.1	<0.1
Bi	61.12	60.28	100.46	100.29	99.28	99.19
S	19.54	19.35	<0.1	<0.1	<0.1	<0.1
Formulae						
Cu	1.02	1.01	0.01	0.00	0.01	0.00
Sb	0.00	0.02	0.00	0.00	0.00	0.00
Bi	0.97	0.97	0.99	1.00	0.99	1.00
S	2.03	2.02	0.00	0.00	0.00	0.00

able to natural assemblages, commonly precipitates from hydrothermal solutions at temperatures below the melting point. Above 271°C, native bismuth is formed as liquid droplets, which retain this morphology when solidified (Godovikov and Kolonin, 1966). The radial fractures surrounding most of the dendritic Bi aggregates in the Bieber samples result from expansion of the Bi upon cooling. A significant change of the linear expansion coefficient of pure Bi metal occurs at ~75°C (Godovikov and Kolonin, 1966), which provides a minimum temperature estimate for the Bieber Co-Ni-Bi ore assemblages. In addition, formation temperatures below 300°C are indicated by the presence of emplectite as the major Bi sulphide mineral associated with native bismuth. Experimental studies of the Cu-Fe-Bi-S system show that emplectite is stable at temperatures below 320°C, where inversion to the high-temperature phase cuprobismuthite occurs (Sugaki et al., 1981; Wang, 1994). Very low S concentrations detected in niccolite (<0.1 wt.%) and maucherite (0.2 wt.%) from the Bieber Co-Ni-Bi ores also indicate temperatures well below 300°C. At 300°C, niccolite can accommodate as much as 5.0 wt.% NiS, whereas the maximum sulphur content of maucherite is only 2.0 wt.% at 700°C. The solid-solution relationships of niccolite and maucherite in the Ni-As-S system show a strong decrease of S substitution into both minerals with decreasing temperature (Yund, 1962). The temperature estimates (100−300°C) obtained for the Bieber Co-Ni-Bi ores are in good agreement with the typical temperature range of different styles of post-Variscan mineralization in Central Europe. Systematic fluid inclusion studies (e.g.

Behr et al., 1987; Lüders and Möller, 1992; Behr et al., 1993; Muchez et al., 1994; Kling, 1997) have demonstrated that most of the post-Variscan vein-type mineralizations (e.g. Pb-Zn-fluorite-baryte veins widespread in Central Europe) have formed in a narrow temperature interval between 100 and 200°C; only a few data show slightly higher temperatures, up to 300°C.

Mechanisms of ore deposition

Most of the conceptual models developed for the post-Variscan vein-type baryte-Pb-Zn mineralization in Central Europe invoke deposition of baryte as a consequence of mixing between deep-sourced metal-bearing basement brines and cooler sulphate-rich formation waters. The sulphate-rich formation waters were probably derived from Permian or Mesozoic carbonate rocks, which contain abundant intercalations of anhydrite (e.g. Behr et al., 1987; Lüders et al., 1993; Zheng and Hoefs, 1993). Recent studies have shown that the precipitation of sulphide minerals in these vein systems is probably related to thermochemical sulphate reduction processes during interaction of the hydrothermal fluids with organic matter in the wallrocks (Jochum, 2000). The distinct spatial association of the Co-Ni-Bi enrichments in the Bieber veins with the sedimentary rocks of the Kupferschiefer (both vertically and laterally) suggests a genetic link between the mineralization style and this particular host-rock lithology. The abundant organic matter in the Kupferschiefer could have acted as a reducing agent for dissolved oxidized sulphur and arsenic species in the hydrothermal fluids, which would have resulted in the

deposition of Co-Ni arsenides and sulpharsenides in close vicinity to the contact between the basement rocks and the Kupferschiefer. A model of thermochemical reduction of arsenites and sulphates was originally proposed by Blair (1997) to explain the unusual mineral assemblages, the geological setting and the structural distribution of the classical Co-Ni-Bi-Ag-As (five-element) veins of Cobalt, Ontario. In a series of reduction experiments carried out with arsenite- and sulphate-bearing hydrothermal solutions at temperatures of 200°C and 300°C, Ni-Co sulpharsenides were precipitated, together with native silver and Ag_2S (Blair, 1997). The results of these experiments suggest that the process of thermochemical arsenite reduction is likely to occur under favourable conditions in ore-forming environments. Experimental studies and analytical data from active geothermal systems demonstrate that arsenic is predominantly transported as oxidized As(III) species in ore-forming fluids, such as $H_3AsO_3^0$, $H_2AsO_3^-$, $HAsO_3^{2-}$ and AsO_3^{3-}, whereas As(V) species are only found in oxidizing near-surface environments (e.g. Ballantyne and Moore, 1988; Krupp and Seward, 1990; Akinfiyev et al., 1992; Pokrovski et al., 1996; Wood and Samson, 1998). Similarly, the deep-sourced thermal spring system at the southern margin of the Rhenish Massif, Germany, which can be considered as a modern analogue of the basement-derived post-Variscan mineralizing fluids, contains significant concentrations of As(III) species (Schwenzer et al., 2001). The experimental and analytical evidence, combined with the lithological and structural setting of the Bieber Co-Ni-Bi ore deposits, make it plausible that thermochemical reduction processes as a consequence of interaction between metal-bearing hydrothermal fluids and the organic-rich hostrocks of the Kupferschiefer resulted in the deposition of Co-Ni-arsenides, Co-Ni sulpharsenides and native Bi.

Age of mineralization

Although no direct radiometric dating of the Co-Ni-Bi assemblage has been carried out, the available age data (Hautmann et al., 1999) from multiple-stage vein mineralization in the nearby Sailauf rhyolite complex can be used to place some constraints on the timing of the Bieber deposit. The mineralization sequence of the Sailauf rhyolite comprises a complex succession of Fe and Mn oxides/carbonates and arsenates as well as different generations of white mica. The relative age relationships between different generations of Fe-Mn oxides and the major generation of baryte in the Spessart district (corresponding to baryte I of the Bieber deposit) have been established, based on detailed textural investigation. Manganite and a first generation of braunite predate the deposition of tabular baryte, which has been subsequently overgrown by specularitic hematite and hausmannite. The onset of mineralization in the vein systems of the Sailauf rhyolite was at 178−180 Ma (illite, K-Ar), whereas several stages of deposition of oxide minerals and micas have been dated between 161 and 98 Ma (Hautmann et al., 1999), using K-Ar (illite, celadonite) and (U+Th)-He chronometry (oxides). The first generation of braunite (pre-baryte) has an (U+Th)-He age of 157−161 Ma, whereas the specularitic hematite (post-baryte) has been dated at 136−148 Ma; hausmannite yields an age of ~130 Ma (Hautmann et al., 1999). Taking these radiometric age data as a basis, the onset of hydrothermal mineralization in the baryte veins of the Spessart (including the Bieber deposit) must have occurred at ~150−160 Ma. The duration of the hydrothermal activity is presently unknown, but the observed multiple brecciation and deposition events indicate repeated hydrothermal pulses. The minimum age obtained from comparison with the radiometric data of the mineralization in the Sailauf rhyolite coincides well with other radiometric ages of post-Variscan vein-type mineralization styles in Central Europe. Several recent studies show that extensional tectonic movements during the Triassic to Late Jurassic were accompanied by strong hydrothermal activity (e.g. Halliday and Mitchell, 1984; Haack and Lauterjung, 1993; Hagedorn and Lippolt, 1993; Wernicke and Lippolt, 1995, 1997a, 1997b). The framework of available radiometric age data allows us to place the formation of the Bieber Co-Ni-Bi deposit into a common model of Mesozoic mineralization in Central Europe.

(University of Würzburg) is thanked for support during XRD work.

References

Akinfiyev, N.N., Zotov, A.V. and Nikonorov, A.P. (1992) Thermodynamic analysis of equilibria in the system As(III)-S(II)-O-H. *Geochemistry International*, **29**, 109–121.

Ballantyne, J.M. and Moore, J.N. (1988) Arsenic geochemistry in geothermal systems. *Geochimica et Cosmochimica Acta*, **52**, 475–483.

Bayliss, P. (1969) X-ray data, optical anisotropism, and thermal stability of cobaltite, gersdorffite, and ullmannite. *Mineralogical Magazine*, **37**, 26–33.

Bechtel, A. and Püttmann, W. (1991) The origin of the Kupferschiefer-type mineralization in the Richelsdorf Hills, Germany, as deduced from stable isotope and organic geochemical studies. *Chemical Geology*, **91**, 1–18.

Behr, H.J., Horn, E.E., Frentzel-Beyme, K. and Reutel, C. (1987) Fluid inclusion characteristics of the Variscan and post-Variscan mineralizing fluids in the Federal Republic of Germany. *Chemical Geology*, **61**, 273–285.

Behr, H.J., Gerler, J., Hein, U.F. and Reutel, C.J. (1993) Tectonic Brines und Basement Brines in den mitteleuropäischen Varisziden: Herkunft, metallo-genetische Bedeutung und geologische Aktivität. *Göttinger Arbeiten zur Geologie Paläontologie*, **58**, 3–28.

Blair, T. (1997) *Thermochemical arsenite reduction (TAR): A new hypothesis for the origin of "Cobalt-type" Ni-Co-arsenide vein deposits*. Thesis, McGill University, Canada, 38 pp.

Diederich, G. and Laemmlen, M. (1964) Das obere Biebertal im Nordspessart. Neugliederung des Unteren Buntsandsteins, Exkursionsführer und geologische Karte. *Geologisches Jahrbuch Hessen*, **48**, 34 pp.

Dobbe, R.T.M. and Oen, I.S. (1994) The polymetallic Cu-Co ores in the central mineralized zone at Tunaberg, Bergslagen, Sweden. *Neues Jahrbuch für Mineralogie Abhandlungen*, **166**, 261–294.

Fleet, M.E. (1972) The crystal structure of pararammelsbergite (NiAs$_2$). *American Mineralogist*, **57**, 1–9.

Freymann, K. (1991) Der Metallerzbergbau im Spessart. Ein Beitrag zur Montangeschichte des Spessarts. *Veröffentlichungen des Geschichts- und Kunstvereins Aschaffenburg*, **33**, 413 pp.

Gerlach, R. (1992) Kluftgebundene Mineralisationen im subsalinaren Tafeldeckgebirge des Harzvorlandes – Lagerstättentyp Mansfelder Rücken. *Zeitschrift für geologische Wissenschaften*, **20**, 233–238.

Godovikov, A.A. and Kolonin GR (1966) Experi-

mentelle Untersuchungen der Bildungsbedingungen von Wismut und die Möglichkeiten seiner Benutzung als geologisches Thermometer. *Zeitschrift für Angewandte Geologie*, **12**, 128–130.

Haack, U. and Lauterjung, J. (1993) Rb/Sr dating of hydrothermal overprint in Bad Grund by mixing lines. Pp. 103–113 in: *Formation of Hydrothermal Vein Deposits – a Case Study of the Pb–Zn, Barite and Fluorite Deposits of the Harz Mountains* (P. Möller and V. Lüders, editors). Monograph Series on Mineral Deposits, **30**. Borntraeger, Berlin.

Hagedorn, B. and Lippolt, H.J. (1993) Isotopic age constraints for epigenetic mineralizations in the Harz mountains (Germany) from K-Ar, ^{40}Ar/^{39}Ar and Rb-Sr data of authigenic K-feldspars. Pp. 87–102 in: *Formation of Hydrothermal Vein Deposits – a Case Study of the Pb-Zn, Barite and Fluorite Deposits of the Harz Mountains* (P. Möller and V. Lüders, editors). Monograph Series on Mineral Deposits, **30**. Borntraeger, Berlin.

Halliday, A.N. and Mitchell, J.G. (1984) K-Ar ages of clay-size concentrates from the mineralization of the Pedroches Batholith, Spain, and evidence for Mesozoic hydrothermal activity associated with the breakup of Pangaea. *Earth and Planetary Science Letters*, **68**, 229–239.

Hautmann, S., Brander, H., Lippolt, H.J. and Lorenz, J. (1999) K-Ar and (U+Th)-He chronometry of multi-stage alteration and mineralisation in the Hartkoppe rhyolite, Spessart, Germany. *Journal of Conference Abstracts*, **4**, 769.

Hofmann, R. (1979) Die Entwicklung der Abscheidungen in den gangförmigen, hydrothermalen Barytvorkommen Mitteleuropas. Pp. 81–214 in: *Zur Minerogenie des hydrothermalen Baryts in Deutschland*. *Monograph Series on Mineral Deposits*, **17**. Borntraeger, Berlin.

Ixer, R.A., Stanley, C.J. and Vaughan, D.J. (1979) Cobalt-, nickel-, and iron-bearing sulpharsenides from the north of England. *Mineralogical Magazine*, **43**, 389–395.

Jochum, J. (2000) Variscan and post-Variscan lead-zinc mineralization, Rhenish Massif, Germany: evidence for sulfide precipitation via thermochemical sulfate reduction. *Mineralium Deposita*, **35**, 451–464.

Kautzsch, E. (1953) Tektonik und Paragenese der Rücken im Mansfelder und Sangerhäuser Kupferschiefer. *Geologie*, **1**, 3–24.

Klemm, D. (1965*a*) Untersuchung mit der Elektronenstrahlmikrosonde über die natürlichen Mischkristallbereiche der Skutterudite. *Contributions to Mineralogy and Petrology*, **11**, 322–333.

Klemm, D. (1965*b*) Synthesen und Analysen in den Dreiecksdiagrammen FeAsS-CoAsS-NiAsS und FeS$_2$-CoS$_2$-NiS$_2$. *Neues Jahrbuch für Mineralogie Abhandlungen*, **103**, 205–255.

Kling, M. (1997) Genesis of the ankerite-siderite-baryte deposit of Kamsdorf (Thuringia, Germany): Fluid inclusion, Sr- and stable isotope constraints. Pp. 535−537 in: *Mineral Deposits: Research and Exploration, Where do they Meet?* (H. Papunen, editor). Proceedings of the 4th biennial SGA meeting, Turku.

Krupp, R.E. and Seward, T.M. (1990) Transport and deposition of metals in the Rotokawa geothermal system, New Zealand. *Mineralium Deposita*, **25**, 73−81.

Lorenz, J. (1991) Die Mineralien im Rhyolith von Sailauf − eine Ergänzung. *Aufschluss*, **42**, 1−38.

Lorenz, J. (1995) Mineralisationen aus dem Rhyolith-Steinbruch von Sailauf einschließlich der Neufunde von ged. Arsen, Bertrandit, Humboldtin und Tilasit. *Aufschluss*, **46**, 105−122.

Lüders, V. and Möller, P. (1992) Fluid evolution and ore deposition in the Harz Mountains (Germany). *European Journal of Mineralogy*, **4**, 1053−1068.

Lüders, V., Gerler, J., Hein, U.F. and Reutel, C.J. (1993) Chemical and thermal development of ore-forming solutions in the Harz Mountains: a summary of fluid inclusion studies. Pp. 117−132 in: *Formation of Hydrothermal Vein Deposits − a Case Study of the Pb−Zn, Barite and Fluorite Deposits of the Harz Mountains* (P. Möller and V. Lüders, editors). Monograph Series on Mineral Deposits, **30**. Borntraeger, Berlin.

Matthes, S. and Okrusch, M. (1965) Spessart. Sammlung geologischer Führer, vol. 44. Borntraeger, Berlin, 220 pp.

Muchez, P., Slobodnik, M., Viaene, W. and Keppens, E. (1994) Mississippi Valley-type Pb-Zn mineralization in eastern Belgium: Indications for gravity-driven flow. *Geology*, **22**, 1011−1014.

Murawski, H. (1954) Bau und Genese von Schwerspatlagerstätten des Spessart. *Neues Jahrbuch für Geologie Paläontologische Monatshefte*, 145−163.

Oen, I.S., Dunn, P.J. and Kieft, C. (1984) The nickel-arsenide assemblage from Franklin, New Jersey; description and interpretation. *Neues Jahrbuch für Mineralogie Abhandlungen*, **150**, 259−272.

Petruk, W., Harris, D.C. and Stewart, J.M. (1971) Characteristics of arsenides, sulpharsenides and antimonides. *Canadian Mineralogist*, **11**, 150−186.

Pokrovski, G., Gout, R., Schott, J., Zotov, A. and Harrichouri, J.C. (1996) Thermodynamic properties and stoichiometry of As(III) hydroxide complexes at hydrothermal conditions. *Geochimica et Cosmochimica Acta*, **60**, 737−749.

Radcliffe, D. and Berry, L.G. (1968) The safflorite-loellingite solid solution series. *American Mineralogist*, **53**, 1856−1881.

Ramdohr, P. (1981) *The Ore Minerals and their Intergrowths*. Pergamon Press, Oxford, 1207 pp.

Rentzsch, J. and Knitzschke, G. (1968) Die Erzmineralparagenesen des Kupferschiefers und ihre regionale Verbreitung. *Freiberger Forschungsh.*, **C231**, 189−211.

Roseboom, L. (1962) Skutterudites (Co,Ni,Fe)As$_{3-x}$: composition and cell dimensions. *American Mineralogist*, **47**, 310−327.

Roseboom, L. (1963) Co-Fe-Ni diarsenides: composition and cell dimension. *American Mineralogist*, **48**, 271−299.

Rosner, B. (1970) Untersuchungen mit der Elektronenstrahlmikrosonde an natürlichen Skutteruditen. *Contributions to Mineralogy and Petrology*, **28**, 135−146.

Schmitt, R.T. (1992) Die Grube Hilfe Gottes bei Großkahl im Spessart. *Aufschluss*, **43**, 309−318.

Schmitt, R.T. (1993*a*) Sulfide und Arsenide aus den Gruben Segen Gottes bei Huckelheim und Hilfe Gottes bei Großkahl im Spessart. *Aufschluss*, **44**, 111−122.

Schmitt, R.T. (1993*b*) Wismutminerale aus den Barytgängen des Spessarts. *Aufschluss*, **44**, 329−336.

Schwenzer, S.P., Tommaseo, C.E., Kersten, M. and Kirnbauer, T. (2001) Speciation and oxidation kinetics of arsenic in the thermal springs of Wiesbaden spa, Germany. *Fresenius Journal of Analytical Chemistry*, **371**, 927−933.

Speczik, S. (1995) The Kupferschiefer mineralization of central Europe: New aspects and major areas of future research. *Ore Geology Reviews*, **9**, 411−426.

Sugaki, A., Kitakaze, A. and Hayashi, K. (1981) Synthesis of minerals in the Cu-Fe-Bi-S system under hydrothermal condition and their phase relations. *Bulletin de Mineralogie*, **104**, 484−495.

Sun, Y. and Püttmann, W. (1997) Metal accumulation during and after deposition of the Kuferschiefer from the Sangerhausen basin, Germany. *Applied Geochemistry*, **12**, 577−592.

Sun, Y. and Püttmann, W. (2000) The role of organic matter during copper enrichment in Kupferschiefer from the Sangerhausen basin, Germany. *Organic Geochemistry*, **31**, 1143−1161.

Tobschall, H.J., Schmidt, F.P. and Schumacher, C. (1986) Exkursion C 2; Kupferschiefer und Kupfervererzungen im Richelsdorfer Gebirge, Hessen; Ihre Entstehung im Rahmen der sedimentären Entwicklung des basalen Zechsteins. *Fortschritte der Mineralogie*, **64**, 2, 143−160.

Vaughan, D.J., Sweeney, M., Friedrich, G., Diedel, R. and Haranczyk, C. (1989) The Kupferschiefer: An overview with an appraisal of the different types of mineralization. *Economic Geology*, **84**, 1003−1027.

Wang, N. (1994) The Cu-Bi-S system: results from low-temperature experiments. *Mineralogical Magazine*,

58, 201−204.

Weber, K. (1995) The Spessart Crystalline Complex. Pp. 167−173 in: *Pre-Permian Geology of Central and Eastern Europe* (R. Dalmeyer, W. Franke and K. Weber, editors). Springer, Berlin.

Wernicke, R.S. and Lippolt, H.J. (1995) Direct isotope dating of a Northern Schwarzwald qtz-ba-hem vein. *Neues Jahrbuch für Mineralogie Monatshefte*, 161−172.

Wernicke, R.S. and Lippolt, H.J. (1997*a*) (U+Th)-He evidence of Jurassic continuous hydrothermal activity in the Schwarzwald basement, Germany. *Chemical Geology*, **138**, 273−285.

Wernicke, R.S. and Lippolt, H.J. (1997*b*) Evidence of Mesozoic multiple hydrothermal activity in the basement of Nonnenwattweiher (southern Schwarzwald), Germany. *Mineralium Deposita*, **32**, 197−200.

Wood, S.A. and Samson, I.M. (1998) Solubility of ore minerals and complexation of ore metals in hydrothermal solutions. *Reviews in Economic Geology*, **10**, 33−76.

Wrobel, P.L. (2000) *Postcollisional lamprophyres and hydrous basaltic dykes from the Mid German Crystalline Rise: resolution of the effects of mantle metasomatism, wedge depletion, melting degree,* *fractionation and crustal assimilation*. PhD thesis, University of Würzburg, Germany, 180 pp.

Yund, R.A. (1962) The system Ni-As-S; phase relations and mineralogical significance. *American Journal of Science*, **260**, 761−782.

Zakrzewski, M.A., Burke, E.A.J. and Nutgeren, H.W. (1980) Cobalt minerals in the Hällefors area, Bergslagen, Sweden: new occurrences of costibite, paracostibite, nisbite and cobaltian ullmannite. *The Canadian Mineralogist*, **18**, 165−171.

Zheng, Y.F. and Hoefs, J. (1993) Stable isotope geochemistry of hydrothermal mineralizations in the Harz Mountains. II. Sulfur and oxygen isotopes of sulfides and sulfate and constraints on metallogenic models. Pp. 211−229 in: *Formation of Hydrothermal Vein Deposits − a Case Study of the Pb-Zn, Barite and Fluorite Deposits of the Harz Mountains*. Monograph Series on Mineral Deposits, **30**. Borntraeger, Berlin.

Ziegler, P.A. (1987) Late Cretaceous and Cenozoic intra-plate compressional deformation in the Alpine foreland − a geodynamic model. *Tectonophysics*, **137**, 389−420.